


# Green's function Monte Carlo method combined with restricted Boltzmann machine approach to the frustrated $J_1$–$J_2$ Heisenberg model

He-Yu Lin(林赫羽), Rong-Qiang He(贺荣强), and Zhong-Yi Lu(卢仲毅)
**Citation:**Chin. Phys. B, 2022, 31 (**8**): 080203. DOI: 10.1088/1674-1056/ac615f
Journal homepage: http://cpb.iphy.ac.cn; http://iopscience.iop.org/cpb

**What follows is a list of articles you may be interested in**

---

## Ionospheric vertical total electron content prediction model in low-latitude regions based on long short-term memory neural network

Tong-Bao Zhang(张同宝), Hui-Jian Liang(梁慧剑),Shi-Guang Wang(王时光), and Chen-Guang Ouyang(欧阳晨光)
Chin. Phys. B, 2022, 31 (**8**): 080701. DOI: 10.1088/1674-1056/ac4487

## Memristor-based multi-synaptic spiking neuron circuit for spiking neural network

Wenwu Jiang(蒋文武), Jie Li(李杰), Hongbo Liu(刘洪波), Xicong Qian(钱曦聪), Yuan Ge(葛源), Lidan Wang(王丽丹), and Shukai Duan(段书凯)
Chin. Phys. B, 2022, 31 (**4**): 040702. DOI: 10.1088/1674-1056/ac380b

## Differentiable programming and density matrix based Hartree-Fock method

Hong-Bin Ren(任宏斌), Lei Wang(王磊), and Xi Dai(戴希)
Chin. Phys. B, 2021, 30 (**6**): 060701. DOI: 10.1088/1674-1056/abeeed

## Restricted Boltzmann machine: Recent advances and mean-field theory

Aurélien Decelle, Cyril Furtlehner
Chin. Phys. B, 2021, 30 (**4**): 040202. DOI: 10.1088/1674-1056/abd160

## Quantum Monte Carlo study of hard-core bosons in Creutz ladder with zero flux

Yang Lin(林洋), Weichang Hao(郝维昌), Huaiming Guo(郭怀明)
Chin. Phys. B, 2018, 27 (**1**): 010204. DOI: 10.1088/1674-1056/27/1/010204

---

# Green's function Monte Carlo method combined with restricted Boltzmann machine approach to the frustrated $J_1$–$J_2$ Heisenberg model

He-Yu Lin(林赫羽), Rong-Qiang He(贺荣强)[†], and Zhong-Yi Lu(卢仲毅)[‡]

*Department of Physics, Renmin University of China, Beijing* 100872, *China*

(Received 17 February 2022; revised manuscript received 23 March 2022; accepted manuscript online 28 March 2022)

Restricted Boltzmann machine (RBM) has been proposed as a powerful variational ansatz to represent the ground state of a given quantum many-body system. On the other hand, as a shallow neural network, it is found that the RBM is still hardly able to capture the characteristics of systems with large sizes or complicated interactions. In order to find a way out of the dilemma, here, we propose to adopt the Green's function Monte Carlo (GFMC) method for which the RBM is used as a guiding wave function. To demonstrate the implementation and effectiveness of the proposal, we have applied the proposal to study the frustrated $J_1$–$J_2$ Heisenberg model on a square lattice, which is considered as a typical model with sign problem for quantum Monte Carlo simulations. The calculation results demonstrate that the GFMC method can significantly further reduce the relative error of the ground-state energy on the basis of the RBM variational results. This encourages to combine the GFMC method with other neural networks like convolutional neural networks for dealing with more models with sign problem in the future.

**Keywords:** restricted Boltzmann machine, Green's function Monte Carlo, frustrated $J_1$–$J_2$ Heisenberg model

**PACS:** 02.70.Ss, 07.05.Mh, 75.10.Jm, 73.43.Nq **DOI:** 10.1088/1674-1056/ac615f

## 1. Introduction

In recent years, machine learning (ML) has been extensively used in physics.[1–4] In Ref. [5], it was proposed to represent the wave functions of quantum many-body systems by a neural network — the restricted Boltzmann machine (RBM).[6] And the transverse Ising and Heisenberg models were then studied. The obtained ground-state energies can be more accurate than the ones by state-of-the-art numerical algorithms. The RBM was also shown to be capable of describing the long-range correlations of quantum systems.[7] Other studies for representing the ground states of one- and two-dimensional models with the RBM variational ansatz[8–10] showed that it could describe ground states and low-lying excited states accurately.

Despite the RBM can perform well for a number of quantum many-body models, it is demonstrated that there are limitations on its expressive ability as a shallow neural network.[11] Here, we propose to adopt the Green's function Monte Carlo (GFMC) method[12,13] to improve the expressive ability of the RBM architecture. The purpose of this paper is to present an investigation in which we implement the GFMC based on an RBM guiding wave function preliminarily optimized by the variational Monte Carlo (VMC) method, here referred to simply as GFMC+RBM method, and then explore its effectiveness.

Considering that the quantum Monte Carlo method is subject to a severe sign problem when applied to the frustrated $J_1$–$J_2$ Heisenberg model on a square lattice, we thus take this model to demonstrate the effectiveness of the GFMC+RBM method. We deliberately benchmark the implemented GFMC+RBM method on a small square lattice with exact diagonalization method, considering its validity, efficiency, and accuracy. Then, for a $6\times 6$ square lattice, we make comparisons of the ground-state energies between the GFMC+RBM method and the pure RBM to illustrate the performance of the method. Finally, we show the spin structure factors of the two methods to determine whether the GFMC+RBM method can capture physical properties of the system.

## 2. Model, method, and implementation

The frustrated $J_1$–$J_2$ Heisenberg model is a typical model with sign problem, which is defined by the following Hamiltonian:

$$H = J_1 \sum_{\langle i,j\rangle} \boldsymbol{S}_i \cdot \boldsymbol{S}_j + J_2 \sum_{\langle\langle i,j\rangle\rangle} \boldsymbol{S}_i \cdot \boldsymbol{S}_j, \tag{1}$$

where $\boldsymbol{S}_i$ $(S = 1/2)$ is a spin operator at site $i$ on a square lattice, $\langle\cdots\rangle$ and $\langle\langle\cdots\rangle\rangle$ indicate pairs of the nearest and next-nearest neighbour sites, respectively.

In this paper, we set $J_1 = 1$. When $J_2 = 0$, the system is in a Neel antiferromagnetic (AFM) long-range order.[14,15] And when $J_2 \gg J_1$, the system is in a well established collinear AFM state.[16,17] The intermediate regime $J_2/J_1 \approx 0.5$ is

[†]Corresponding author. E-mail: rqhe@ruc.edu.cn
[‡]Corresponding author. E-mail: zlu@ruc.edu.cn

© 2022 Chinese Physical Society and IOP Publishing Ltd 

a phase transition regime with high frustration. Although there have been a lot of studies about characteristics of this regime,[18–21] till now a definitive conclusion has not been established.

Properties of the phase transition are charaterized by the spin structure factor which is defined as follows:

$$S^2(\boldsymbol{k}) = \frac{1}{N(N+2)} \sum_{i,j} \langle \boldsymbol{S}_i \cdot \boldsymbol{S}_j \rangle \, \mathrm{e}^{\mathrm{i}\boldsymbol{k}\cdot(\boldsymbol{r}_i - \boldsymbol{r}_j)}, \tag{2}$$

where $\boldsymbol{r}_i$ is the position vector at site $i$, and $\boldsymbol{k}$ is a momentum, $N$ is the total number of spins in the system.

When $\boldsymbol{k} = (0,\pi)$ or $(\pi,0)$, $S^2(\boldsymbol{k}) \neq 0$ implies that the system is in a collinear AFM order.[16,17] Likewise, when $\boldsymbol{k} = (\pi,\pi)$, we can estimate a Neel AFM order based on whether or not $S^2(\boldsymbol{k}) \neq 0$.

Next, we discuss structure and properties of the RBM variational wave function. Previous theoretical works[22,23] have established that as long as a higher-dimensional function is smooth enough and normalized, it can be well approximated by a neural network, and RBMs are capable of representing the wave functions of certain quantum many-body systems approximately.

The RBM is a kind of shallow neural network constituted by a visible layer and a hidden layer, as shown in Fig. 1. The "restricted" means that the neurons belonging to two different layers are coupled with each other, but there is no coupling within the visible or hidden layer themselves. The RBM variational expression reads

$$F_{\mathrm{rbm}}(\boldsymbol{v}) = \sum_{\{h\}} \exp\left( \sum_i a_i v_i + \sum_j b_j h_j + \sum_{i,j} w_{i,j} h_j v_i \right), \tag{3}$$

where the visible neurons and hidden neurons are expressed as $\boldsymbol{v}_i$ and $\boldsymbol{h}_j$, and $\boldsymbol{a} = \{a_i\}$ and $\boldsymbol{b} = \{b_j\}$ represent biases of the visible and hidden layer, respectively, and $\boldsymbol{w} = \{w_{i,j}\}$ are weights which couple the visible and hidden units.

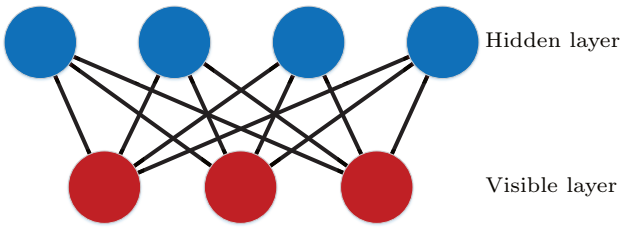



**Fig. 1.** The architecture of the restricted Boltzmann machine. The blue dots in the upper layer denote the hidden neurons, and the red dots in the bottom layer represent the visible neurons.

Since there is no coupling between the auxiliary hidden neurons, the hidden variables can be traced out. The RBM variational wave function thus reads

$$\begin{aligned} F_{\mathrm{rbm}}(\boldsymbol{v}) &= \exp\left( \sum_i v_i a_i \right) \times \sum_{\{h\}} \prod_j \exp\left[ \sum_i W_{ij} v_i h_j + h_j b_j \right] \\ &= \exp\left( \sum_i v_i a_i \right) \times \prod_j (1 + \exp\theta_j), \end{aligned} \tag{4}$$

where $\theta_j \equiv \sum_i W_{ij} v_i + b_j$ and $v_i$, $h_i = 0$ or 1.

Then we train the variational parameters by minimizing the expectation value

$$E_0 = \langle H \rangle = \frac{\langle F_{\mathrm{rbm}} | H | F_{\mathrm{rbm}} \rangle}{\langle F_{\mathrm{rbm}} | F_{\mathrm{rbm}} \rangle}.$$

In each iteration of the optimization process, we use variational Monte Carlo (VMC) method to sample spin configurations according to such a distribution of $|F_{\mathrm{rbm}}(\boldsymbol{v})|^2$, where $v_i = 0$ for spin down and $v_i = 1$ for spin up. And the optimization method adopted here is the stochastic reconfiguration (SR) method.[13,24,25]

Now, we set forth the basic principles of the GFMC method, which is essentially a stochastic algorithm to perform the power method. The GFMC method is in principle capable of capturing ground-state features of quantum many-body systems.[12,13]

For an initial state $\Psi_0$, as long as it is not orthogonal to the ground state $\Gamma_0$, after a long enough imaginary-time propagation with $\beta_{\mathrm{total}}$, the ground state will be projected out,

$$\lim_{\beta_{\mathrm{total}} \to \infty} \mathrm{e}^{-\beta_{\mathrm{total}} H} |\Psi_0\rangle \propto |\Gamma_0\rangle. \tag{5}$$

In practice, equation (5) is realized by iteratively applying $\Psi(x', \beta_0 + \Delta\beta) = \sum_x G_{x',x} \Psi(x, \beta_0)$ for $M$ times, where $G_{x',x} = \langle x' | \, \mathrm{e}^{-\Delta\beta H} \, | x \rangle$ is the so-called Green's function with $\sum_x |x\rangle\langle x| = 1$. And $\Delta\beta = \beta_{\mathrm{total}}/M$ is a short imaginary time. When $M$ is large enough, the above formula can be approximated as $G_{x',x} \approx \langle x' | \, 1 - \Delta\beta H \, | x \rangle$.

The evolution process is considered as a random process, and the Green's function can be directly interpreted as a probability transition matrix. But, generally $\sum_{x'} G_{x',x} \neq 1$, we thus divide $G_{x',x}$ into the product of two factors $G_{x',x} = p_{x',x} b_x$, where $b_x = \sum_{x'} G_{x',x}$ is the normalization factor, and the random matrix $p_{x',x} = G_{x',x}/b_x$ is considered as the transition probability of a Markov chain.

The evolution of the wave function can be obtained through a simple Markov process that is defined by $(x, w)$, which is named as a walker. This Markov process is described as follows:

(i) Transform a configuration $x$ into $x'$ with probability $p_{x',x}$.

(ii) Update the weight with $w' = w b_x$.

Then after a large enough imaginary-time propagation, the system converges to an equilibrium distribution corresponding to the ground state. And the ground-state energy can be thus obtained by statistically averaging the results of $n$ independent evolutions, with $n$ being large enough. For each independent simulation, setting the starting weight as $w_0 = 1$, the accumulated weight of each projection process with $p$ steps

is $G_n^p = \prod_{j=1}^{p} b_{x_j}$. The statistical average for the ground-state energy is calculated by the accumulated weight

$$E_0 \approx \frac{\sum_n G_n^p e_{\mathrm{L}}(x_n)}{\sum_n G_n^p},$$

where $e_{\mathrm{L}}(x_n) = \sum_{x'} H_{x',x_n}$. The total imaginary-time length is $\beta_{\mathrm{total}} = p\beta$, $\beta$ being the evolution time of a single Markov step which usually consists of several $\Delta\beta$. $\beta_{\mathrm{total}}$ needs to be large enough to ensure that the projection process can reach the ground-state wave function.

For a Monte Carlo method, we usually adopt the importance sampling to guide the sampling process. After a thermalization time, configuration $x$ will distribute with probability $|\Psi_{\mathrm{g}}|^2$, $\Psi_{\mathrm{g}}$ is a guiding function of the importance sampling. In this work, we employ an RBM variational function as the guiding function (A comprehensive comparison with random initial states as a guiding function is given in Appendix A).

Since the GFMC method is essentially a random process, the off-diagonal elements of $G_{x',x}$ must be non-negative, otherwise there is a sign problem. We adopted the fixed-node approximation[26–28] to circumvent the sign problem and we don't go into detail in this paper.

For the GFMC method, its guiding wave function needs to be real. But, for the model studied in this work, the RBM guiding wave function has to be complex. We thus need to transform it from complex space to real space, namely, to identify its global complex phase and remove it. To do so, we employ the principal component analysis (PCA).[29,30]

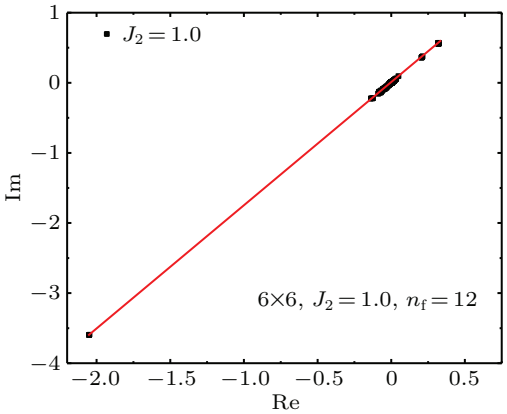



**Fig. 2.** The principal component of the variational wave function of the frustrated $J_1$–$J_2$ Heisenberg model on a $6 \times 6$ square lattice with $J_2 = 1.0$. The black squares denote the results of the variational wave function corresponding to different configurations, and there are $2 \times 10^4$ black squares in the figure. The principal component represent by the red line.

The PCA is a type of variable reduction method which is adopted to analyze datasets described by several intercorrelated variables. This method can effectively extract important information from a dataset, then represent it as a set of new orthogonal variables defined as principal components. In this work, we utilize the PCA method to extract the principal component of the guiding wave functions so as to reduce the wave functions from the complex space to the real space.

As shown in Fig. 2, we consider the frustrated $J_1$–$J_2$ Heisenberg model on a $6 \times 6$ square lattice with $J_2 = 1.0$. Sampling a large number of configurations, the corresponding results of the variational representation are shown by the black squares in the complex coordinate system. And the principal component is represent by the red line. The projections of the values of the variational wave function on the principal component axis are the new real wave functions.

## 3. Results

With its implementation, we first benchmark the GFMC+RBM method by exact diagonalization method on a $4 \times 4$ square lattice.

Figure 3 shows the dependence of the ground-state energy on the total imaginary-time $\beta_{\mathrm{total}}$ on a $4 \times 4$ square lattice. With the increase of $\beta_{\mathrm{total}}$, the ground-state energies calculated by the GFMC decrease gradually from the one given by the RBM until they reach the exact value. For three different single Markov step length $\beta$, we all get the same result.

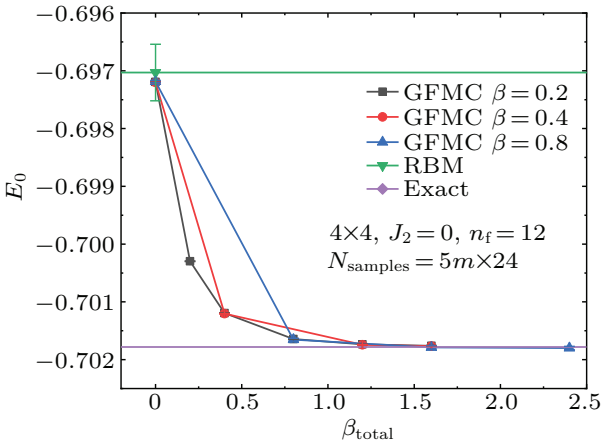



**Fig. 3.** The ground-state energy as a function of the imaginary-time $\beta_{\mathrm{total}}$ on a $4 \times 4$ square lattice with three different $\beta$. $\beta_{\mathrm{total}}$ is the total evolution time, and $\beta$ represents the evolution time for a single Markov step. $n_{\mathrm{f}}$ is the ratio of the number of hidden units to visible units for the architecture of the RBM guiding wave function.

Next, we employ the GFMC+RBM method to study the frustrated $J_1$–$J_2$ Heisenberg model on a $6 \times 6$ square lattice. The obtained relative errors and spin structure factors are shown in Figs. 4 and 5 respectively. Here the relative error is defined as $|(E - E_{\mathrm{exact}})/E_{\mathrm{exact}}|$, where $E_{\mathrm{exact}}$ is the exact value of the ground state energy. The spin structure factor is defined by Eq. (2).

As shown in Fig. 4, in comparison with the RBM, the GFMC+RBM method substantially reduces the relative errors of the ground state energies. One notices that the relative errors decrease significantly away from the transition region.

The GFMC+RBM method performs in the phase transition region not as well as it does in the non-phase transition regions. It is well known that the characteristics of the phase transition region are still controversial due to the competing orders in this region. Actually, the variational results of the RBM get larger errors in this region, the RBM as a guiding wave function is thus not sufficiently precise for the GFMC, then leading to larger errors for the GFMC as well in the phase transition region. This suggests to find a neural network with stronger expressibility instead of the RBM serving as a better guiding wave function for the GFMC.

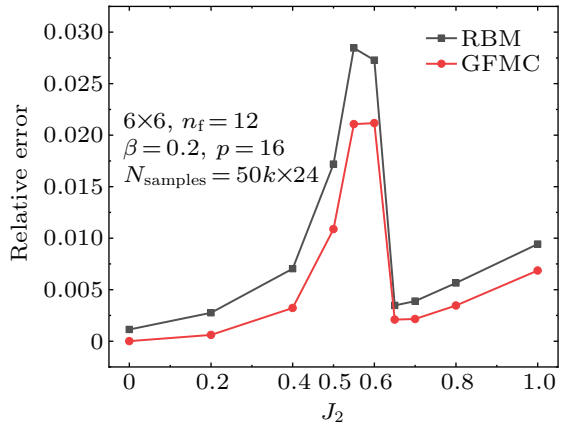



**Fig. 4.** The relative errors of the RBM and GFMC+RBM method results for the frustrated $J_1$–$J_2$ Heisenberg model on a $6 \times 6$ square lattice. The vertical axis represents the relative errors $|(E - E_{exact})/E_{exact}|$, the exact results are taken from the Ref. [31], and the number of filters of RBM is $n_f = 12$.

Figure 5 shows the phase transition diagram on a $6 \times 6$ square lattice with different $J_2$ values. The vertical axis represents the spin structure factor. For $\boldsymbol{k} = (\pi, \pi)$, the calculation results are shown as the black dots, and the spin structure factor can be used to indicate whether or not there is a Neel phase transition. A Neel AFM order exists in the system when $J_2 < 0.45$, while it gradually disappears for $J_2 > 0.5$. The range of $0.45 < J_2 < 0.70$ is a phase transition region. Similarly, the spin structure factor for $\boldsymbol{k} = (\pi, 0)$ can be used to indicate the existence of a collinear AFM phase, and the results are shown in the figure with red dots.

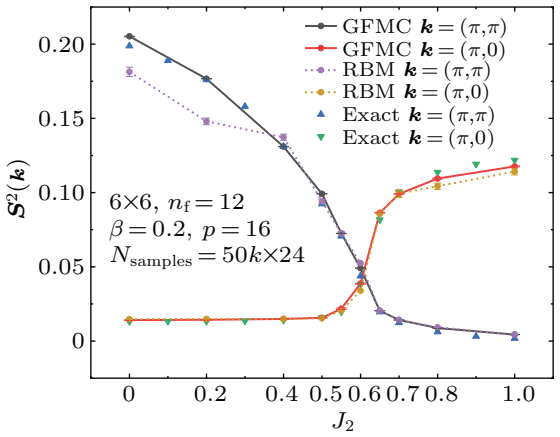



**Fig. 5.** The spin structure factors of frustrated $J_1$–$J_2$ Heisenberg model on a $6 \times 6$ square lattice. The error bars represent the statistical errors of the GFMC method.

Figure 6 shows the spin structure factors calculated on a $10 \times 10$ square lattice. The detailed calculation results of $6 \times 6$ and $10 \times 10$ square lattice are listed in Tables 1 and 2, respectively.

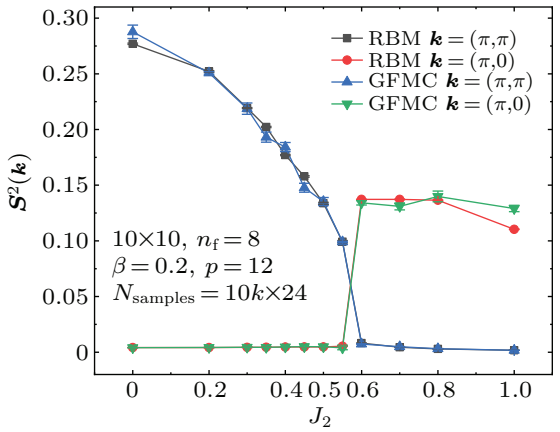



**Fig. 6.** Spin structure factors of frustrated $J_1$–$J_2$ Heisenberg model on a $10 \times 10$ square lattice. The error bars represent the statistical errors of the GFMC method.

**Table 1.** Comparison between the RBM and RBM+GFMC method relative errors of ground state energies. The last row is the ratio between them. The exact energies on a $6 \times 6$ square lattice are taken from Ref. [31].

| $6 \times 6$ | $J_2 = 0.0$ | $J_2 = 0.2$ | $J_2 = 0.4$ | $J_2 = 0.5$ | $J_2 = 0.55$ | $J_2 = 0.6$ | $J_2 = 0.8$ | $J_2 = 1.0$ |
|---|---|---|---|---|---|---|---|---|
| Exact | −0.678872 | −0.599046 | −0.529745 | −0.503810 | −0.495178 | −0.493239 | −0.586487 | −0.714360 |
| RBM relative error | 0.00189 | 0.00369 | 0.00631 | 0.01555 | 0.02173 | 0.01122 | 0.00573 | 0.00955 |
| GFMC relative error | $4.7137 \times 10^{-5}$ | $9.9492 \times 10^{-4}$ | 0.0035 | 0.01062 | 0.01811 | 0.0088 | 0.00341 | 0.00654 |
| Ratio | 40.12812 | 3.70839 | 1.79984 | 1.46385 | 1.19976 | 1.27531 | 1.68141 | 1.46053 |

**Table 2.** Comparison of ground-state energies between the RBM and GFMC+RBM method on a $10 \times 10$ square lattice.

| $10 \times 10$ | $J_2 = 0.0$ | $J_2 = 0.2$ | $J_2 = 0.4$ | $J_2 = 0.45$ | $J_2 = 0.5$ | $J_2 = 0.55$ | $J_2 = 0.6$ | $J_2 = 0.8$ | $J_2 = 1.0$ |
|---|---|---|---|---|---|---|---|---|---|
| RBM | −0.66652(1) | −0.58712(1) | −0.51487(1) | −0.49610(1) | −0.48339(1) | −0.46865(1) | −0.46541(1) | −0.56613(1) | −0.68487(1) |
| GFMC+RBM | −0.67004(1) | −0.59039(1) | −0.51901(1) | −0.5010(1) | −0.48741(1) | −0.47359(1) | −0.4690(1) | −0.5702(1) | −0.6901(1) |

## 4. Summary

In this paper, we implemented the combination of the GFMC method and the RBM to study the frustrated $J_1$–$J_2$ model on a square lattice. Taking the variational result of the RBM as a guiding wave function for the GFMC, we calculated the ground state energies and spin structure factors of the model with different $J_2$ on a $6\times6$ square lattice, and then compared the results between the GFMC+RBM method and the pure RBM method. The GFMC + RBM method improves the accuracy of the ground state energies. And the spin structure factors given by the GFMC + RBM method are also better than those of the pure RBM method. Similar conclusion can be obtained in the study for a $10\times10$ square lattice. Overall, the GFMC+RBM method well outperforms the RBM. It is very instructive to combine the RBM and GFMC method to study quantum systems with sign problem. This encourages to replace the RBM wave function with other neural networks with stronger expressibility like CNN on more challenging models in the future.

## Appendix A: The comprehensive comparison between the RBM and random initial states

We carried out the calculations and made a comprehensive comparison between the random initial states and the RBM. We show that for the GFMC the RBM as a guiding wave function well outperforms the random initial states as guiding wave functions.

We prepared the random initial states by setting up the RBM with randomly generated network parameters so that the RBM gives random wave functions, whose nodal surfaces are hence also random and whose energies are around zero and far above the true ground state energies. As the following tables show, for both $4\times4$ and $6\times6$ square lattices and for both $J_2=0$ and 0.55, when the random states are used respectively as a guiding wave function, the GFMC can only slightly reduce the energies and the minimized energies are still far above the exact ground state energies. As a contrast, when the variationally optimized RBM states used respectively as a guiding wave function, the minimized energies are close to the exact ones, showing that the variationally optimized RBM states possess a meaningful nodal surface and well outperform the random initial states.

**Table A1.** Ground state energies for the frustrated $J_1$–$J_2$ model on the $4\times4$ square lattice, $n_f=2$, $\beta_{\text{total}}=6.4$, $N_{\text{samples}}=5m\times24$.

| | $J_2=0.0$ | $J_2=0.55$ |
|---|---|---|
| RBM (random) | 0.31665(1) | 0.49795(1) |
| GFMC+RBM (random) | −0.17749(1) | −0.00882(4) |
| RBM (optimized) | −0.69712(1) | −0.48770(3) |
| GFMC+RBM (optimized) | −0.70179(1) | −0.50567(1) |
| Exact | −0.701780 | −0.523595 |

**Table A2.** Ground state energies for the frustrated $J_1$–$J_2$ model on the $6\times6$ square lattice, $n_f=12$, $\beta_{\text{total}}=6.4$, $N_{\text{samples}}=50k\times24$.

| | $J_2=0.0$ | $J_2=0.55$ |
|---|---|---|
| RBM (random) | 0.17215(1) | −0.27724(1) |
| GFMC+RBM (random) | 0.02916(4) | −0.29092(1) |
| RBM (optimized) | −0.67797(1) | −0.48109(1) |
| GFMC+RBM (optimized) | −0.67887(1) | −0.48475(2) |
| Exact | −0.678872 | −0.495178 |

## Acknowledgements

Project supported by the National Natural Science Foundation of China (Grant Nos. 11934020 and 11874421) and the Natural Science Foundation of Beijing (Grant No. Z180013). Computational resources were provided by National Supercomputer Center in Guangzhou with Tianhe-2 Supercomputer and Physical Laboratory of High Performance Computing in RUC.

## References

[1] Carrasquilla J and Melko R G 2017 *Nat. Phys.* **13** 431
[2] Nieuwenburg E, Liu Y H and Huber S D 2017 *Nat. Phys.* **13** 435
[3] Schindler F, Regnault N and Neupert T 2017 *Phys. Rev. B* **95** 245134
[4] Venderley J, Khemani V and Kim E A 2018 *Phys. Rev. Lett.* **120** 257204
[5] Carleo G and Troyer M 2017 *Science* **355** 602
[6] Hinton G E 2002 *Neural Computation* **14** 1771
[7] Deng D L, Li X and Sarma S D 2017 *Phys. Rev. X* **7** 021021
[8] Nomura Y, Darmawan A S, Yamaji Y and Imada M 2017 *Phys. Rev. B* **96** 205152
[9] Chen J, Cheng S, Xie H, Wang L and Xiang T 2018 *Phys. Rev. B* **97** 085104
[10] Glasser I, Pancotti N, August M, Rodriguez I D and Cirac J I 2018 *Phys. Rev. X* **8** 011006
[11] Gao X and Duan L M 2017 *Nat. Commun.* **8** 662
[12] Anderson J B 1975 *J. Chem. Phys.* **63** 1499
[13] Becca F and Sorella S 2017 *Quantum Monte Carlo Approaches for Correlated Systems* (London: Cambridge University Press) p. 167
[14] Calandra Buonaura M and Sorella S 1998 *Phys. Rev. B* **57** 11446
[15] Sandvik A W 1997 *Phys. Rev. B* **56** 11678
[16] Neel L 1936 *Annales de Physique* **11** 232
[17] Neel L 1932 *J. Phys. Radium* **3** 160
[18] Wang L, Poilblanc D, Gu Z C, Wen X G and Verstraete F 2013 *Phys. Rev. Lett.* **111** 037202
[19] Liu W Y, Dong S, Wang C, Han Y, An H, Guo G C and He L 2018 *Phys. Rev. B* **98** 241109
[20] Hu W J, Becca F, Parola A and Sorella S 2013 *Phys. Rev. B* **88** 060402
[21] Gong S S, Zhu W, Sheng D N, Motrunich O I and Fisher M P A 2014 *Phys. Rev. Lett.* **113** 027201
[22] Hornik K 1991 *Neural Network* **4** 251
[23] Roux N L and Bengio Y 2008 *Neural Computation* **20** 1631
[24] Sorella S 1998 *Phys. Rev. Lett.* **80** 4558
[25] Casula M and Sorella S 2003 *J. Chem. Phys.* **119** 6500
[26] Sorella S and Capriotti L 2000 *Phys. Rev. B* **61** 2599
[27] Reynolds P J, Ceperley D M, Alder B J and Lester W A 1982 *J. Chem. Phys.* **77** 5593
[28] Haaf D T, Bemmel H V, Leeuwen J V, Van S and Ceperley D 1995 *Phys. Rev. B* **51** 13039
[29] Wold S, Esbensen K and Geladi P 1987 *Chemometrics and Intelligent Laboratory Systems* **2** 37
[30] Abdi H and Williams L J 2010 *Wiley Interdisciplinary Reviews: Computational Statistics* **2** 433
[31] Schulz H, Ziman T and Poilblanc D 1996 *Journal de Physique I* **6** 675